THE ASTROPHYSICAL JOURNAL, Vol. 150, December 1967

GALACTIC H II REGIONS. III. THE NATURE OF THE RADIO SOURCE W49

P. G. MEZGER AND J. SCHRAML
National Radio Astronomy Observatory*
AND
YERVANT TERZIAN
Arecibo Ionospheric Observatory†

Received March 30, 1967; revised June 8, 1967

ABSTRACT

The galactic radio source W49 is one of two associations of thermal sources, nonthermal sources, and OH-emission clouds found in an earlier survey of the free-free continuum and H109α recombination line radiation of twenty galactic radio sources. In this paper the nature of W49 is investigated using the results of high angular resolution continuum observations in the frequency range 195 MHz $\leq \nu \leq$ 15 4 GHz. W49 consists of a thermal component A (G43.2+0 0) and a non-thermal component B (G43 3−0.2). Both components are nearly at the same distance, 14.1 kpc, from the sun and at a distance of about 10 kpc from the galactic center. The projected distance between the centers of components A and B is 12′.5 or 51 pc If the non-thermal component B is a supernova remnant, it must be a considerably older and originally a much more powerful supernova remnant than Cassiopeia A.

Both the analysis of the spectrum and the high angular resolution observations of the brightness temperature distribution of the radio continuum of the thermal component A suggest that it consists of several high density condensations, A2, of small size ($2R < 1$ pc) and high density ($N_0 > 10^4$ cm^{-3}) which are imbedded in a component, A1, of lower electron density ($N_0 = 234$ cm^{-3}) and larger diameter ($2R = 14.4$ pc). It needs from six to eleven O5 stars to ionize component A2. These high-density condensations may be the ionized shells (cocoons) of recently formed stars, whose existence has been predicted by Davidson and Harwit.

Non-thermal emission of the 18-cm OH-lines close to W49 comes from two emission centers which are closely associated in space with the thermal component A. The OH-emission centers seem to coincide with the position of the thermal high-density condensations A2; this indicates a close correlation between star formation and non-thermal OH emission.

The total thermal component A is surrounded by a shell of neutral hydrogen, for which an upper limit of 3.2×10^5 solar masses of H I is obtained. Shell and H II-regions together form a gravitationally stable system, which could be the early stage of an O- and B-star association. The non-thermal component B, probably an old supernova remnant, is located at the outer edge of the shell of neutral hydrogen.

I. INTRODUCTION

The radio continuum and recombination line emission of twenty galactic sources have been recently investigated at a frequency of 5 GHz (Mezger and Henderson 1967; Mezger and Höglund 1967, cited hereafter as "Paper I" and "Paper II," respectively). It was found that the giant H II regions G43.2+0.0 in W49 and G49.0−0.3 and G49.5−0.4 in W51 are associated with both non-thermal continuum sources and OH clouds which show a strong, non-thermal emission of 18-cm lines.

In this paper we investigate one of these associations, W49, in more detail. In addition to the observational results given in Papers I and II, we use new continuum observations made with telescopes of high angular resolution in the frequency range 195 MHz $\leq \nu \leq$ 15.4 GHz.

W49 was first detected by Westerhout (1958) during his 22-cm survey. When observed with an angular resolution of 10′ or better, W49 is clearly resolved into two components (Fig. 1). The components are separated in α by 12′.5 and have nearly the same

* The National Radio Astronomy Observatory, Green Bank, West Virginia is operated by Associated Universities, Inc., under contract with the National Science Foundation.

† The Arecibo Ionospheric Observatory, Arecibo, Puerto Rico, is operated by Cornell University with the support of the Advanced Research Projects Agency under a research contract with the Air Force Office of Scientific Research.

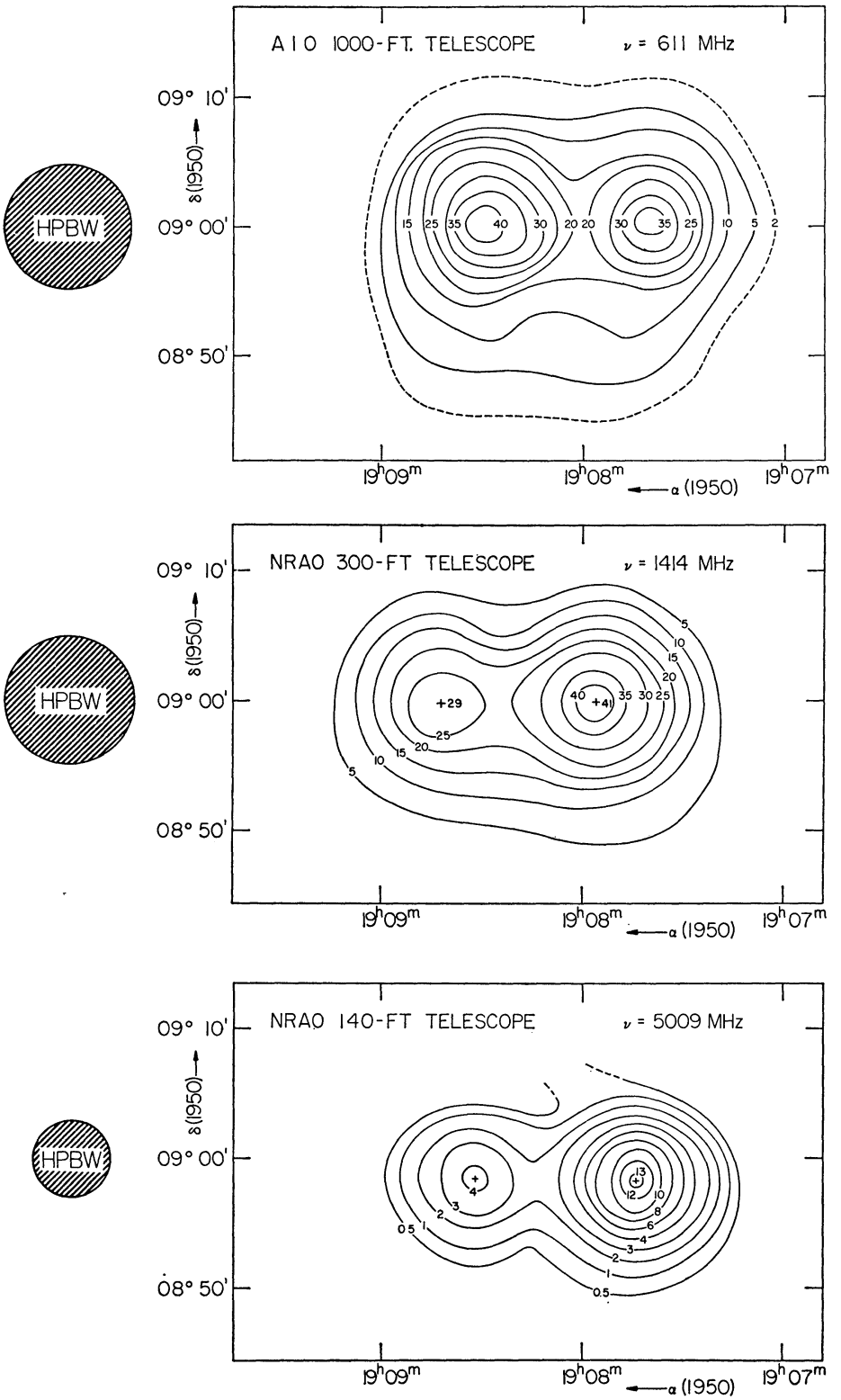

FIG. 1.—Contour maps of W49, measured at three different frequencies with the AIO 1000-foot telescope and the NRAO 300-foot and 140-foot telescopes, respectively. One contour unit corresponds to a brightness temperature of the source averaged over the antenna main beam of 10° K at 611 MHz, 2.45° K at 1414 MHz and 1.24° K at 5009 MHz. The 611 MHz contours should be shifted by $+12^s$ in α. Positions are not corrected for systematic pointing errors.

declination. From their recombination line spectra, it was deduced that component G43.2+0.0 is a thermal source (H II region) and component G43.3−0.2 is a non-thermal source. Table 1 summarizes the results pertaining to the two components of W49 which were derived in Papers I and II.

The bottom line of this table refers to the corresponding tables in Papers I and II from which the numerical values have been taken. The physical parameters of the thermal component, given in the seventh through the tenth columns, have been derived by adopting a uniform spherical density distribution of the hydrogen plasma. The electron temperature given in the eleventh column has been computed on the assumption that the plasma is optically thin in the continuum. Its value $T_e = 6300°$ K is only slightly higher than the average electron temperature ($\langle T_e \rangle = 5800°$ K) of fifteen spiral-arm H II regions (Paper II, § IV). However, the rms velocity of internal turbulence, given in the twelfth column of Table 1, is considerably smaller than the average value of $\langle v_t(\text{rms}) \rangle = 19.3$ km sec^{-1} of the same fifteen spiral-arm H II regions (Paper II, § VI).

OH lines are found in non-thermal emission close to the thermal component of W49. Interferometer observations (Rogers, Moran, Crowther, Burke, Meeks, Ball, and Hyde 1967) show two distinct emission centers of very small angular size. From observations of the 1665 MHz line, one distinguishes thirteen OH clouds with different radial velocities (Weaver, Dieter, and Williams 1966). The difference of the radial velocity between the 109α recombination line emitted by the H II region G43.2+0.0, and the mean value of the radial velocities of the associated thirteen OH clouds is given in the thirteenth column. The velocity dispersion between the OH clouds and the H II region, given in the last column, is of the same order as the velocity dispersion of clouds of interstellar neutral or ionized hydrogen. Statistical evaluation of the radial velocities of OH clouds and nearby H II regions has led to the conclusion that OH clouds and H II regions do not accidentally coincide in their positions, but are in fact closely correlated in space (Paper II, § IX).

II. OBSERVATIONS AND THEIR REDUCTION

At the lowest frequencies, 81.5 and 178 MHz, flux density measurements made at the Mullard Observatory, Cambridge, England (Shakeshaft, Ryle, Baldwin, Elsmore, and Thomson 1955; Bennett 1962) are used in our analysis. At 195, 430, and 611 MHz our observations were made with the Arecibo Ionospheric Observatory (AIO) 1000-foot telescope. The observations at these frequencies were reduced using a procedure similar to that described by Terzian (1965). At 750 and 1414 MHz, observations were made with the NRAO 300-foot telescope. Besides our own measurements, we have used independent observations by Pauliny-Toth, Wade, and Heeschen (1966). At frequencies of 2.7 GHz and higher, we used the NRAO 140-foot telescope. The calibration of the NRAO telescopes in all our observations is based on the high-frequency spectra of Taurus A and Virgo A given by Baars, Mezger, and Wendker (1965).[1] It should be emphasized that in the frequency range $\nu > 750$ MHz most flux density and position measurements are cross-checked by two independent observations, made in different observing periods and by different observers. In addition, 7.8 GHz observations by Burke and Wilson (1967) were available, obtained with the Haystack 120-foot telescope.

The major source of error in the determination of the flux density of W49 (and of galactic sources in general) arises from the uncertainty in the separation of the source and background radiation. Observational experience tells us that the unresolved galactic

[1] Since the spectral analysis by Baars *et al.* was published (1965), new absolute and relative flux density measurements have been published. An unpublished reanalysis of the spectra which includes these new data shows that the predicted flux density values for frequencies > 10 GHz have to be slightly decreased. We used these revised flux density values for the calibration of the 140-foot telescope Calibration sources and adopted flux densities are given in the ninth column of Table 2, for all unpublished flux density measurements.

TABLE 1

PHYSICAL PARAMETERS OF THE TWO COMPONENTS G43.2+0.0 AND G43.3−0.2 OF W49 (AS DERIVED IN PAPERS I AND II)

1967ApJ...150..807M

Component	Radiation Mechanism	θ_α	θ_δ	$\theta_G = \sqrt{(\theta_\alpha \theta_\delta)}$	Distance (kpc)	$2R$ (pc)	N_e (cm^{-3})	$M/M\odot$	E_{max} (pc cm^{-6})	T_e (° K)	$\langle V_t^2 \rangle_{rms}$ (km/sec)	V_r(H II) − $\langle V_r(OH) \rangle$ (km/sec)	$\langle [V_r(OH) - V_r(H\ II)]^2 \rangle_{rms}$ $\langle V_r(OH) \rangle$ (km/sec)
G43.2+0.0	H II-region	3′.4	2′.8	3′.1	14.1	18.7	180	15230	6.1×10^5	6300	14.5	−6.8	9.3
G43.3−0.2	Supernova remnant?	4′.2	4′.0	4′.1	?	.	.	.	.	.		.. ..	. . .
Given in Paper	II, Table 1	I, Table 3			II, Table 2	I, Table 5				II, Table 2		II, Table 5	

disk component varies only slowly with galactic longitude. Hence, to separate the source from the background, we stacked the α-drift curves observed at the source and adjacent declinations and drew a lower envelope of the stacked cross-sections. This was considered the brightness temperature distribution of the unresolved galactic background, which was then subtracted from the observed cross-section. Figure 1 shows representative contour maps which were obtained with the AIO 1000-foot telescope and the NRAO 300-foot and 140-foot telescopes. Flux density and position values used in the following analysis are compiled in Table 2.

In the cases where the two components were not clearly resolved, we have listed positions and flux density values under W49 in the second and fifth columns. At 1175 MHz it was only possible to determine the relative contribution of the two components to the total flux density.

For the sake of simplicity, we have designated in the following discussion the thermal component G43.2+0.0 as component A, the non-thermal component G43.3−0.2 as component B. To obtain their accurate positions, we have taken the average value of the positions given in the third and fourth columns of Table 2. This leads to the values given in Table 3.

The spectra of the integrated flux density of $W49$ ($S_A + S_B$) and of the two components A and B separately (S_A and S_B, respectively) are shown in Figure 2. The flux density values with their error limits are taken from Table 2. Between 700 MHz and 15 GHz the spectrum of the non-thermal component can be approximated by a straight line (corresponding to a spectral index $\alpha = -0.41$).

At the lowest frequencies the positions of the integrated source $W49$ (second column of Table 2) agree, within the error limits, with the position of the non-thermal component B. From this we conclude that at frequencies below 200 MHz the contribution of the thermal component A to the integrated flux density of W49 is negligible. The integrated flux density values below 200 MHz and the flux density values of component B observed at 430 and 611 MHz can be approximated by another straight line, which corresponds to a spectral index of $\alpha = -0.17$. The two straight spectra of component B intersect at approximately 650 MHz. The spectrum S_A of the thermal component will be discussed in the following section.

III. A MODEL OF THE THERMAL COMPONENT A (G43.2+0.0) OF W49

Separate flux density measurements of the two components of W49 are available for frequencies $\nu \geq 430$ MHz. As discussed in the preceding section, a linear extrapolation of the spectrum S_B toward lower frequencies seems to be justified. The low-frequency part of spectrum S_A, shown as a dashed curve in Figure 2, was consequently obtained by subtracting S_B fron the integrated spectrum $S_A + S_B$. The resulting spectrum S_A decreases rapidly at frequencies below 700 MHz and has maxima at about 1.4 and 9 GHz.

To interpret this spectrum, we have considered a homogeneous sphere of hydrogen plasma with the apparent diameter $\theta_{sph} = 2R/D$, with $2R$ the linear diameter of the sphere and D its distance from the Sun. If we assume a constant electron temperature of the plasma, the flux density emitted by this spherical H II region at the frequency ν is given by

$$S_\nu = \frac{2k\nu^2}{c^2} T_e \int (1 - e^{-\tau_c})\, d\Omega . \tag{1}$$

Here k is the Boltzmann constant and c the velocity of light. For the spherical density distribution, equation (1) has the two limiting approximations

$$S_\nu' = \frac{2k\nu^2}{c^2} \frac{\pi}{4} \theta^2_{sph} T_e \qquad \text{(valid for } \bar{\tau}_c \gg 1\text{)} \tag{2a}$$

TABLE 2

Flux Densities and Positions of W 49 and Its Components A (G 43.2 + 0.0) and B (G 43.3 - 0.2)

1	2a	2b	3a	3b	4a	4b	5	6	7	8	9a	9b	10
	Positions (1950)						Flux Density S_ν				Telescope Calibration		
ν/MHz	W 49		G 43.2 + 0.0		G 43.3 - 0.2		x 10^{-26} Wm^{-2} Hz^{-1}			Epoch	Calibration Source	Flux Density x 10^{-26} Wm^{-2} Hz^{-1}	References *
	α	δ	α	δ	α	δ	W 49	G 43.2+0.0	G 43.3 - 0.2				
81.5	$19^h\ 08^m\ 43^s \pm 5^s$	$+09°\ 23' \pm 60'$					69 ± 13			<1955	---	---	1
178	$19^h\ 08^m\ 44.0^s \pm 1.5$	$+09°\ 00.7' \pm 3'$					55 ± 3			<1962	---	---	2
195	$19^h\ 08^m\ 34^s \pm 7^s$	$+09°\ 01.2' \pm 2'$					57 ± 10			1965.75	3C 386	25	3a
430							76 ± 10	29 ± 4	47 ± 6	1965.75	3C 386	15	3a
611			$19^h\ 07^m\ 52^s \pm 4^s$	$+09°\ 00.5' \pm 1.5'$	$19^h\ 08^m\ 42^s \pm 4^s$	$+09°\ 00.0' \pm 1.5'$	87 ± 10	39 ± 4	48 ± 6	1967.1	3C 386	12	3a
750							91 ± 16	45 ± 8	46 ± 8	1963.8	---	---	4
750	$19^h\ 08^m\ 20.5^s \pm 4^s$	$+09°\ 00.1' \pm 1'$					83 ± 12	40 ± 6	43 ± 6	1966.25	Virgo	349	3b
1175								(56.2 ± 5)%	(43.8 ± 5)%		---	---	3b
1400			$19^h\ 07^m\ 54.9^s \pm 2^s$	$+08°\ 59.2' \pm 0.5'$	$19^h\ 08^m\ 42.9^s \pm 2^s$	$+08°\ 59.8' \pm 0.5'$	79.8 ± 3.1	47.2 ± 1.8	32.6 ± 1.3	1963.8	---	---	4
1414			$19^h\ 07^m\ 55.5^s \pm 3^s$	$+09°\ 00.9' \pm 1'$	$19^h\ 08^m\ 43.5^s \pm 3^s$	$+09°\ 00.1' \pm 1'$	74 ± 7	44 ± 4	30 ± 3	1966.25	Virgo	208	3b
2700	$19^h\ 07^m\ 58^s \pm 6^s$	$+08°\ 59.8' \pm 1.5'$					80^{+3}_{-10}			1965.75	Hydra	21.8	3c
2700	$19^h\ 07^m\ 54^s \pm 6^s$	$+09°\ 01.3' \pm 1.5'$					81^{+4}_{-8}			1966.6	Virgo	123	3c
5000			$19^h\ 07^m\ 44^s \pm 4^s$	$+09°\ 01.7' \pm 1'$	$19^h\ 08^m\ 38.7^s \pm 8^s$	$+09°\ 01.9' \pm 2'$	80 ± 10	57.5 ± 7	22.1 ± 3	1965.65			5
5000							77.7 ± 8	59.8 ± 6	17.9 ± 3	1967.1	Cygnus	375	3c
7830			$19^h\ 07^m\ 52^s \pm 2^s$	$+09°\ 00.3' \pm 0.5'$	$19^h\ 08^m\ 44^s \pm 2^s$	$+09°\ 00.1' \pm 0.5'$	84 ± 10	66 ± 7	18.2 ± 3	1967.0	Virgo	49.7	6
15375			$19^h\ 07^m\ 49^s \pm 4^s$	$+09°\ 01.0' \pm 1'$			79 ± 10	64 ± 7	15 ± 3	1966.25	Taurus	461	3c
15375			$19^h\ 07^m\ 47^s \pm 4^s$	$+09°\ 01.0' \pm 1'$	$19^h\ 08^m\ 37^s \pm 6^s$	$+09°\ 00.4' \pm 1.5'$	67 ± 10	56 ± 7	11 ± 3	1966.75	Taurus	461	3c
15375							68 ± 10	58 ± 7	10 ± 3	1966.9	Cygnus	99	3c

* References are as follows:

(1) Shakeshaft, Ryle, Baldwin, Elsmore and Thomson (1955).
(2) Bennett (1962); Errors in (1) and (2) as quoted by Howard and Maran (1965).
(3) This paper: (3a) Observations performed with AIO 1000-foot telescope. (3b) Observations performed with NRAO 300-foot telescope. (3c) Observations performed with NRAO 140-foot telescope.
(4) Pauliny-Toth, Wade and Heeschen (1966).
(5) Mezger and Henderson (1967).
(6) Burke and Wilson (1967); observations performed with Haystack 120-foot telescope.

and

$$S_\nu'' = \frac{2k\nu^2}{c^2}\frac{\pi}{6}\theta^2_{\rm sph}\bar{\tau}_c T \qquad \text{(valid for } \bar{\tau}_c \ll 1\text{)} \quad (2b)$$

with

$$\bar{\tau}_c = \frac{1}{\Omega_s}\int \tau_c d\Omega = 8.235\times 10^{-2} a(\nu,T_e)\left(\frac{T_e}{^\circ\mathrm{K}}\right)^{-1.35}\left(\frac{\nu}{\mathrm{GHz}}\right)^{-2.1}\left(\frac{E_{\rm center}}{\mathrm{pc\ cm^{-6}}}\right), \quad (3)$$

the mean value of the optical path length of the free-free continuum averaged over the projected sphere. This mean value is equal to the optical path length through the center of the sphere (Appendix A).

Substituting equation (3) in equation (2b), it is found that the flux density of the H II region increases as $S_\nu' \sim \nu^2$ for $\bar{\tau}_c \gg 1$ and decreases approximately as $S_\nu'' \sim \nu^{-0.1}$ for $\bar{\tau}_c \ll 1$. The two approximations intersect at the turnover frequency[2] ν_t, at which $S'(\nu_t) = S''(\nu_t)$ and $\bar{\tau}_c(\nu_t) = \frac{2}{3}$.

[2] Note, however, that the maximum of the flux density of an H II region occurs at the frequency $\nu_{\rm max} \approx 3\nu_t$ where $\bar{\tau}_c(\nu_{\rm max}) \approx 0.1$.

TABLE 3

AVERAGE VALUES OF THE POSITIONS OF THE TWO COMPONENTS IN W49

Component	Designation in This Paper	α(1950)	δ(1950)
G43.2+0.0	A	$19^h07^m50^s.6 \pm 4^s.2$	$09°00'.7 \pm 0'.6$
G43.3−0.2	B	19 08 41.4 ± 2.8	09 00.4 ± 0.8

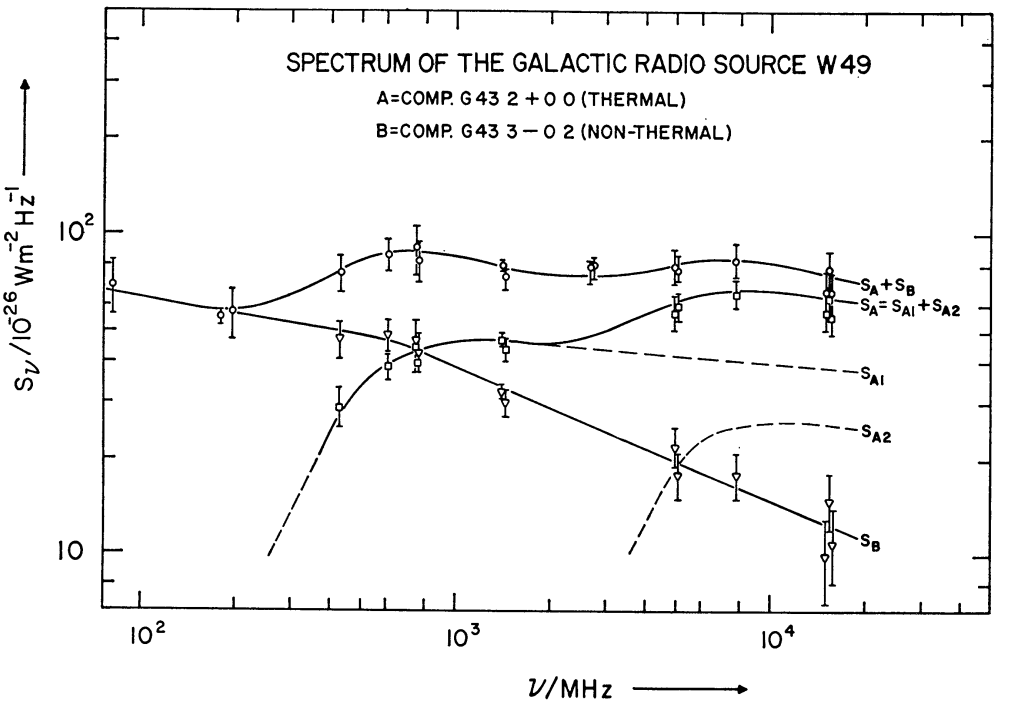

FIG. 2.—Observed integrated spectrum of W49 and observed and interpolated spectra of its components A (G43.2+0.0), A1 and A2, and B (G43.3−0.2).

The corresponding relation for ν_t is given in Appendix A. If the electron temperature is known, the turnover frequency is determined by the emission measure E_{center} only. Close to the turnover frequency the spectrum S_ν of the spherical H II region can be computed from the following equation (Osterbrock 1965):

$$\frac{S_\nu}{S_\nu''} = \frac{3}{\bar{\tau}_c^3}\left[\tfrac{1}{2}\bar{\tau}_c^2 + (1+\bar{\tau}_c)\, e^{-\bar{\tau}_c} - 1\right], \tag{4}$$

which gives that fraction of the free-free flux density which escapes into space. This function is tabulated in Appendix A, Table 6. For $\bar{\tau}_c \gg 1$. equation (4) approaches the limiting value $S_\nu'/S_\nu'' = 3/(2\bar{\tau}_c)$. Equations (2)–(4) allow us to fit models of spherical H II regions to the observed thermal spectrum of component A of W49.

To explain the spectrum S_A in Figure 2, we obviously need two H II regions with considerably different emission measures. A possible model consists of a dense H II region with high emission measure and small apparent diameter (designated in the following as component A2), which is imbedded in an H II region of lower density and emission measure, but larger apparent diameter (designated as component A1). At frequencies below 2 GHz the contribution of the flux density S_{A2} emitted by the high-density component A2 to the total flux S_A of the thermal component can be neglected. Hence, we determine the turnover frequency $\nu_t(\text{A1}) \approx 600$ MHz for the low-density component from the spectrum S_A. At higher frequencies where component A is optically thin, its spectrum can be extrapolated by adopting the spectral law $S_{A1} \sim \nu^{-0.1}$ (shown as dashed curve S_{A1} in Figure 2).

To derive the spectrum of the high-density component A2, we subtract the extrapolated spectrum S_{A1} from the observed spectrum S_A and obtain in this way the dashed curve S_{A2} in Figure 2, which has its turnover frequency at $\nu_t(\text{A2}) \approx 6$ GHz.

Substituting these turnover frequencies in equation (A.2) and adopting an electron temperature $T_e = 6000°$ K, the emission measures given in the fourth column of Table 4 are computed. The emission measure of component A1, $E_{\text{center}} = 7.87 \times 10^5$ pc cm^{-6} lies close to the upper limit found in the brightest diffuse emission nebulae (Paper I, Table 5). The emission measure of component A2, $E_{\text{center}} = 1.02 \times 10^8$ pc cm^{-6}, however, lies about two orders of magnitude above the highest emission measure—E_c (Orion A) $= 2.1 \times 10^6$ pc cm^{-6}—known to date.

The adopted model of a high-density condensation imbedded in an H II region of considerably lower density seems to be able to explain the spectrum S_A of the thermal component of W49. This model even holds for n condensations, as long as they have approximately the same emission measure and do not overlap within the line of sight. Nevertheless, the reality of this model would remain questionable if there were no more direct evidence of the existence of bright emission centers of small apparent diameter in the brightness distribution of the thermal component A.

Such evidence comes from both single dish and interferometer observations. Figure 3 shows the brightness distribution of the thermal and non-thermal components of W49, observed at 15.4 GHz with an angular resolution of 2′. Both components A and B are partly resolved. The thermal component is elongated and may be resolved into two or more components if observed with a sufficiently high angular resolution. Apparently, the average position of component G43.2+0.0, given in Table 3 and indicated in Figure 3, falls somewhere between the two parts of the partially resolved component A2.

Preliminary observations with the NRAO interferometer at 2.7 GHz (Paper I, § V) have shown that component A still has a very complex structure when observed with an angular resolution of 20″, although component A2 contributes, at this frequency, only 10 per cent of the total thermal flux density.

TABLE 4

PHYSICAL PARAMETERS OF THE COMPONENTS A1 AND A2 OF THE H II REGION COMPONENT A (G43.2 + 0.0) OF W49

COMPONENT	ν_t (MHz)	$\alpha(\nu_t)$	E_{center} (pc cm^{-6})	$S_{10\ GHz}$ (f.u.)	$\alpha_{10\ GHz}$	θ_{sph} (rad)	θ_{sph}	$2R$ (pc)	N_0 (cm^{-3})	$M/M\odot$		$RN^{2/3}$ (pc cm^2)
										Ind. Cond.	Total	
A1.												
$n=1$.	600	0.9956	7.87×10^5	40	...	1.02×10^{-3}	3′.52	14.4	2.34×10^2	9.3×10^3	9.3×10^3	273
A2:												
$n=1$.						7.35×10^{-5}	15″.3	1.035	9.92×10^3	143	143	238
$n=2$.	6000	0.9800	1.02×10^8	27	0.9675	5.20×10^{-5}	10″.8	0.73	1.18×10^4	60	120	189
$n=6$.						3.00×10^{-5}	6″.2	0.42	1.55×10^4	15	90	131
$n=11$.						2.21×10^{-5}	4″.6	0.31	1.81×10^4	7.2	79	107

IV. THE PHYSICAL CONDITIONS PREVAILING IN THE THERMAL COMPONENTS A1 AND A2

The following computations are performed for an electron temperature of $T_e = 6000°$ K.[3] Given the emission measure and electron temperature of the two components A1 and A2, their flux densities depend only on their solid source angles Ω_s. Equation (2) can hence be used to compute the apparent diameters θ_{sph} of the H II regions. The corresponding relation, equation (A.3), has been worked out in Appendix A for the case of an optically thin spherical H II region of constant electron density.

At $\nu = 10$ GHz both components are optically thin. The flux densities of components A1 and A2, estimated from the separated spectra in Figure 2, are given in the fifth column of Table 4. The computed apparent diameters are given in the seventh and

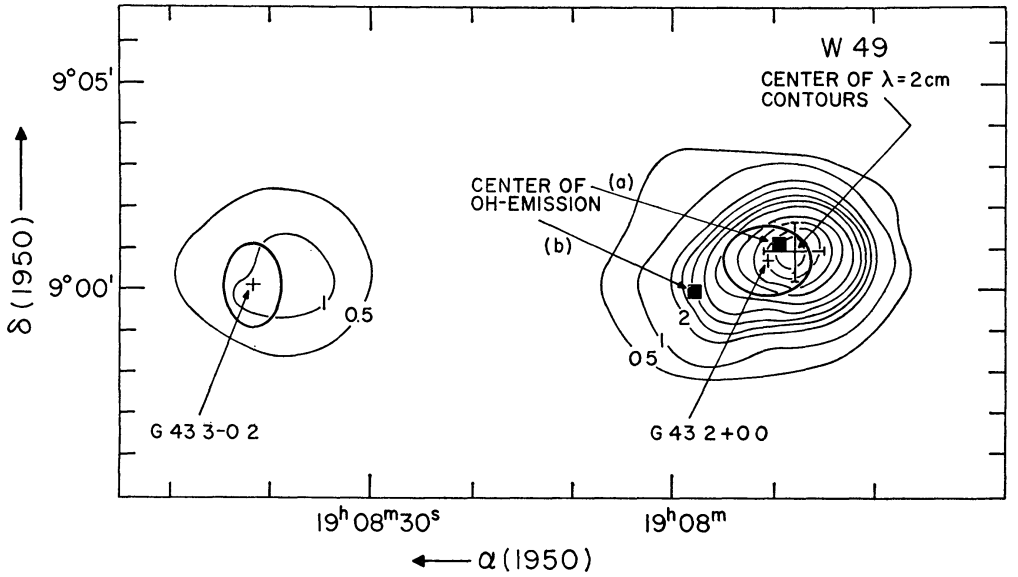

FIG. 3.—Contour map of W49, component A (G43.2+0 0) and component B (G43 3−0.2) observed at 15.4 GHz with an angular resolution of 2′. One contour unit ≙ 0.99° K $\bar{T}_b$ Also given are the average positions of both components, together with their error limits (heavy elliptical contours), the position of the peak values of the 15 4 GHz contour map (with error limits), and the positions of the OH-emission centers (conforming to Rogers *et al.* 1966).

eighth columns. Taking the distance $D = 14.1$ kpc of W49, component A, we obtain the linear diameters in the ninth column. Electron densities and total masses of ionized hydrogen, given in the tenth and eleventh columns of Table 4, have been computed using equations (A.4) and (A.5).

The excitation parameters $s_0 = RN^{2/3}$ (R the radius of the Strömgren sphere and N the electron density) for components A1 and A2 are given in the last column. The large values of the excitation parameters of components A1 and A2 rule out the possibility that either component is ionized by one single main sequence O-type star. We therefore consider in the following computations that component A2 consists of n identical condensations which do not overlap in the line of sight. Observations performed with high angular resolution and discussed in the preceding section strongly support the assumption of the existence of more than one high-density condensation in the thermal component A.

The emission measure RN^2 of component A2 has been determined from the turnover

[3] The dependence of the derived physical parameters on the electron temperature is given by eqs. (A.2)–(A.5). Increasing the electron temperature from 6000° to 9000° K yields: $E_9 = 1.73\ E_6$; $\theta_9 = 0\,82\ \theta_6$; $N_9 = 1.46\ N_6$; and $M_9 = 1\,08\ M_6$.

frequency in the spectrum S_{A2}. It is an observed quantity and must therefore be independent of the number n of condensations. With this condition

$$R(n)N^2(n) = R(n = 1)N^2(n = 1) ,$$

it is found that

$$R(n) = n^{-1/2}R(n = 1) , \quad N_0(n) = n^{1/4}N_0(n = 1) , \quad M_{H\,II}(n) = n^{-5/4}M_{H\,II}(n = 1) .$$

The total mass of n condensations is $nM_{H\,II}(n) = n^{-1/4}M_{H\,II}(n = 1)$. The excitation parameter $s_0 = RN^{2/3}$ becomes

$$s_0(n) = n^{-1/3}s_0(n = 1) .$$

Following Gould, Gold, and Salpeter (1963), an O-type star of visual magnitude $M_v = -6.0$, and with a surface temperature of 55250° K, having a radius of 8.2×10^{11} cm, yields an excitation parameter of 135 pc cm^{-2}. About six of these stars are needed to ionize component A2 in W49.

Since the characteristics of O5 stars are not too well known, we have investigated the excitation parameters of the strongest nearby H II regions, whose bright emission centers seem to be resolved with an angular resolution of 2′. The largest excitation parameter of 106 pc cm^{-2} is found for component G133.7+1.2 of IC 1795. Eleven stars of the type ionizing this H II region are needed to ionize component A2. In Table 4 the physical parameters of the individual condensations are given for $n = 1$, 2, 6, and 11 identical condensations.

Both direct observations and theoretical considerations indicate that component A2 consists of a cluster of high-density condensations imbedded in an extended H II region of lower electron density. The compact H II regions must be very young. A possible explanation for the formation of such high-density H II regions is that a recently formed star has ionized the surrounding dense cloud of hydrogen which was originally needed for the gravitational contraction of the young star. The existence of such "cocoon stars" has been predicted by Davidson and Harwit (1967).

V. NON-THERMAL EMISSION OF THE HYDROGEN 109α AND THE OH LINES

The H109α recombination line emission of W49, component G43.2+0.0, and nineteen other galactic H II regions is discussed in Paper II. The problems involved in the determination of the electron temperatures are discussed in §§ IV and V of that paper. From the measured product of half-power line width times the ratio of center line to free-free continuum temperature, $\Delta\nu_L(T_L/T_C) = 25.6$ kHz, an electron temperature of 6300° K for component A was obtained. The computation is based on the assumption that component A is optically thin. The results in this paper show, however, that the high-density component A2 is still optically thick at 5 GHz (Fig. 2) and therefore should not contribute to the recombination line radiation. The observed recombination line radiation would emit from the low-density component A1 only, and consequently we substitute T_C(A1) rather than T_C(A) for the computation of the electron temperature of component A1. From Figure 2 we estimate S_5(A2) = 19.5 f.u., S_5(A) = 62 f.u., and obtain for the continuum temperature of component A1 T_C(A1) = T_C(A) − T_C(A2) ≈ T_C(A)[1 − S_5(A2)/S_5(A)2] = T_C(A)0.686. This leads to the corrected value $\Delta\nu_L T_L/T_C$(A1) = 25.6/0.686 = 37.3 kHz, which, when substituted in equation (2b) of Paper II, yields an electron temperature of 4500° K for component A1. This value is low in comparison with the average value of 5800° K for all observed spiral arm H II regions. Only in the H II regions W43 (T_e = 3970° K) and W51, component G49.5−0.4 (T_e = 3980° K), are lower electron temperatures found.

It is possible, however, to interpret our observations in a different way. Suppose the electron temperature of the low-density component A1 were close to 6000° K; then the

observed excess line radiation must be emitted by the high-density component A2, in spite of the fact that it is optically thick. This, however, could no longer be a thermal equilibrium radiation but rather an enhanced radiation due to stimulated emission, as has been suggested recently by Goldberg (1966). It is of interest in this connection to note that the two giant H II regions with extremely low electron temperatures mentioned above, when observed with angular resolutions of 2′ ($\lambda = 2$ cm) and 20″ ($\lambda = 11$ cm), show a fine structure in their brightness distribution similar to that of component A of W49. Non-thermal line emission from high-density components imbedded in a hydrogen plasma of lower density could explain why such low electron temperatures are derived for these giant H II regions.

The characteristics of non-thermal OH-emission from regions close to the thermal component A of W49 are summarized in § I of this paper. Recently the position of one of the OH-emission centers has been measured with high accuracy (rms position errors about 5″) using interferometer techniques (Cudaback, Read, and Rougoor 1966; Rogers, Moran, Crowther, Burke, Meeks, Ball and Hyde 1966). The emission center, designated here with (*a*), has the position $\alpha_{1950} = 19^h07^m49.7^s$; $\delta_{1950} = 09°01'12''$.

More recent observations by the latter group (Rogers *et al.* 1967) show a second OH-emission center, designated here by (*b*), whose position is shifted by $\Delta\alpha = +8.5^s$, $\Delta\delta = -68''$ relative to the position of the emission center (*a*). In the 2-cm contour map of W49, components A and B (Fig. 3), the OH-emission centers are shown as filled squares. The position of the OH-emission center (*a*) agrees with the peak of the 2-cm contours within the error limits. The OH-emission center (*b*) lies on the elongated shoulder of the 2-cm brightness temperature distribution; this shoulder might be resolved into a secondary maximum if observed with still higher angular resolution.

In § IV we try to explain the high-density component A2 as an association of very young H II regions which are ionized by O-type stars which were formed only recently. The coincidence of the OH-emission centers with the partially resolved brightest thermal emission centers in component A of W49 suggests a correlation between OH-emission centers and regions of star formation.

This hypothesis is supported by the fact that close to the OH-emission centers in IC 1795/1805 (Mezger, Altenhoff, Schraml, Burke, Reifenstein, and Wilson 1967) and in the Cygnus X region W75/DR 21 (Ryle and Downes 1967; Mezger *et al.* 1967) similar compact H II regions are found which might be in an even earlier stage of evolution than is component A2 in W49. In all these cases the close correlation between the radial velocities of the OH clouds and the hydrogen 109α recombination lines indicates a close spatial correlation between OH-emission centers and very young H II regions. Recent interferometer observations of these OH-emission centers yield an upper limit to their size of 0.″1 but also show that the individual emission centers (as discriminated by their circular polarization and radial velocities, respectively) have slightly different positions (Davies, Rowson, Booth, Cooper, Gent, Adgie, and Crowther 1967). In the case of W49, the possibility cannot be ruled out that the OH-emission centers are located inside the H II region component A1 which has an average electron density of 234 cm^{-3}. The OH clouds might be protostars, whose central cores are not yet hot enough or have been formed too recently to completely ionize the surrounding shell of neutral gas and dust.

VI. THE NON-THERMAL COMPONENT B (G43.3−0.2) IN W49

Based on its recombination line emission, a distance of 14.1 kpc has been estimated for component A (Paper II, Table 2). To estimate the distance of component B, 21-cm line observations are used.

Akabane and Kerr (1965) and, more recently, Sato, Akabane, and Kerr (1967) have made a detailed investigation of the 21-cm line absorption spectrum of W49 with the C.S.I.R.O. 210-foot telescope. They find that component A has a larger optical depth

in the velocity range between 0 and +20 km/s, corresponding to a difference in the numbers of atoms in the line of sight of 3×10^{21} in a 1-cm^2 column. Since this is a typical value for a path length in a spiral arm (assuming an average density of 1 cm^{-3}) Sato *et al.* conclude that the thermal component A and the non-thermal component B are separated by about 1 kpc and are therefore not a physically related double source.

We do not agree with this conclusion for the following reasons:

i) Associations of thermal and non-thermal sources are much more frequent in our Galaxy than was previously thought (Wilson, Reifenstein, Burke, and Mezger 1967). The 21-cm line absorption spectra of one of these associations, W51, have been investigated in detail, and it was found that thermal and non-thermal components are at nearly the same distance (Burton 1966). Hence the probability that thermal component A and non-thermal component B in W49 coincide in the line of sight by accident seems to be fairly low. We prefer to believe that in most cases there exists a physical relation between the non-thermal sources and the associated H II regions.

ii) The thermal component A2 seems to be an ionization limited H II region with an average electron density of 234 cm^{-3} and a diameter of about 14.4 pc. It is highly improbable that the density of the neutral hydrogen surrounding such a dense and massive H II region drops immediately to 1 cm^{-3}, the value adopted by Sato *et al.* A more realistic assumption is that at the ionization front of component A2, the density of the hydrogen plasma and the surrounding neutral hydrogen are at least equal and that the density of the neutral hydrogen then gradually tapers off with increasing distance.

Argument (i) leads us to the conclusion that the true distance between thermal component A and non-thermal component B in W49 is not too different from its projected distance of 51 pc.

Argument (ii) provides us with a model which explains the observed difference in optical depth in the 21-cm line absorption spectra of components A and B. In this model the thermal component A is surrounded by a dense shell of neutral hydrogen which does not extend farther than 50 pc. This model is supported by the fact that Sato *et al* find the maximum difference in optical depth, $\tau_A - \tau_B$, very close to the radial velocity 7.4 km/sec of the recombination line emitted by component A (Paper II, Table 1). With a shell thickness of 40 pc, an average density of $N_{H\,I} = 25$ cm^{-3} is required to account for the observed difference in optical depth. For a uniform density distribution the shell would contain a total amount of 3.2×10^5 solar masses of neutral hydrogen. By adopting a tapered rather than a uniform density distribution, the total mass of neutral hydrogen contained in the shell could be considerably reduced. It is of interest to note, however, that Ebert, von Hoerner, and Temesvary (1960) estimated the radius and total mass of a gravitationally stable O- and B-star association to be 53 pc and 4×10^5 solar masses, respectively.

As a working hypothesis we assume that component B in W49 is a supernova remnant located at the same distance as the thermal component A. In Table 5 and in Figures 4 and 5, some characteristics of component B are compared with the characteristics of Cassiopeia A, a typical galactic supernova remnant. Figure 4 shows the brightness temperature distribution of the two sources, observed with a 2′ beam at 15.4 GHz. The angular scale of the contour map of component B is enlarged by the factor 14.1/3.5 to account for the different distances of the two sources. Likewise, the spectrum of component B in Figure 5 is increased by the factor $(14.1/3.5)^2$. This comparison yields the following: (i) the size of component B is three times larger; (ii) its average surface brightness at 1 GHz is about fifty times weaker, and (iii) its spectrum is considerably flatter than that of Cassiopeia A. These differences indicate that component B in W49 is a rather old object and must have been originally a much more powerful supernova remnant than Cassiopeia A (D. Hogg, personal communication). It is of interest in this connection that the kink in the spectrum of component B occurs at a much lower frequency and is much more pronounced than the kink in the spectrum of Cassiopeia A.

TABLE 5

COMPARISON BETWEEN SOME CHARACTERISTICS OF W49, COMPONENT B (G43 3—0 2) AND CASSIOPEIA A

SOURCE	D (kpc)	⟨HPW⟩ min of arc	⟨HPW⟩ pc	SPECTRAL INDEX	
Cassiopeia A	3 5	4′45	4 5	−0 75 80 MHz≤ν≤3 4 GHz	−0 85 3 4 GHz≤ν≤32 GHz
W49; G43 3—0 2	14 1	3′55	14 5	−0 17 80 MHz≤ν≤650 MHz	−0 41 650 MHz≤ν≤16 GHz

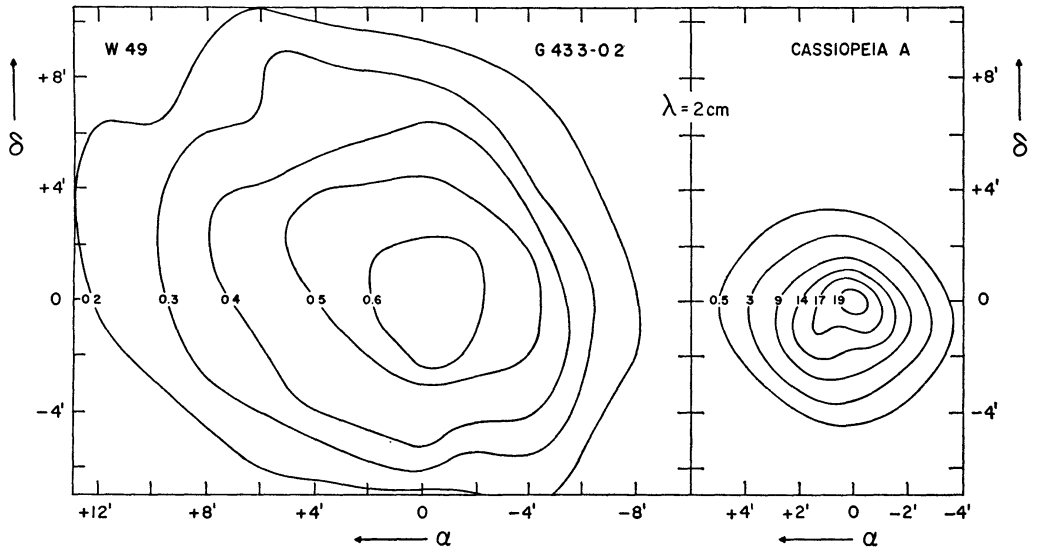

FIG. 4.—Brightness temperature distribution of Cassiopeia A and W49, component B (G43 2—0.2) observed at 15.4 GHz. The contours of component B have been reduced to the same distance as Cassiopeia A. One contour unit ≙ 0 99° K T_b.

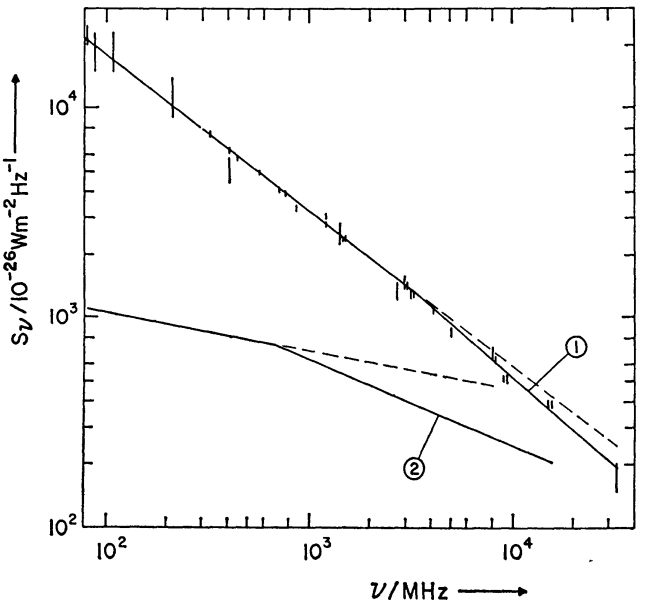

FIG. 5.—Observed spectra of Cassiopeia A and W49, component B (G43 3 — 0 2). The spectrum of component B has been reduced to the same distance as Cassiopeia A.

VII. CONCLUSIONS

The various line and continuum radio observations of the source W49 can be satisfactorily explained by the following model. The thermal component A (G43.2+0.0) is located at a distance 14.1 kpc from the Sun. It consists of a component A1 with a diameter of 14.4 pc, an average density of 234 cm^{-3}, and a total mass of ionized hydrogen of 9.3×10^3 solar masses. Inside this H II region exist several condensations with diameters smaller than 1 pc and electron densities higher than 10^4 cm^{-3}, which together contain about 100 solar masses of ionized hydrogen. These condensations are supposed to be very young H II regions which are ionized by recently formed O-type stars. Close to these condensations are OH clouds which show a strong non-thermal emission of the 18-cm lines. These OH clouds might be protostars in their earliest stages of evolution. The total thermal component A is surrounded by a shell of neutral hydrogen, which may contain as much as 3.2×10^5 solar masses of H I. The whole system is gravitationally stable and could be an early stage of an O- and B-star association. The non-thermal component B of W49 (G43.3−0.2) is a relatively old supernova remnant which is located at the outer edge of the shell of neutral hydrogen.

It is a pleasure to thank F. J. Kerr (C.S.I.R.O., Sydney, Australia), B. F. Burke and T. S. Wilson of Massachusetts Institute of Technology, and A. E. E. Rogers of Lincoln Laboratory, Massachusetts Institute of Technology, for providing us with unpublished data.

APPENDIX

COMPUTATION OF THE PHYSICAL PARAMETERS OF AN H II REGION FROM ITS MEASURED SPECTRUM

In Appendix A of Paper I, formulae were derived which allow the computation of the total mass and electron density of an H II region if its flux density at one frequency, its half-power width (HPW), and its electron temperature are known. Here we have the somewhat different problem that the spectrum of the continuum radiation and the electron temperature of an H II region are known from which we want to determine its HPW, electron density, and total mass of ionized hydrogen.

The optical path length of the free-free continuum radiation of ionized hydrogen is given by equation (A.1a) in Paper I, which can be written in the form

$$\tau_c = 8.235 \times 10^{-2} a(T_e,\nu) \left(\frac{T_e}{^\circ\mathrm{K}}\right)^{-1.35} \left(\frac{\nu}{\mathrm{GHz}}\right)^{-2.1} \left(\frac{E}{\mathrm{pc\ cm^{-6}}}\right), \tag{A.1}$$

with E the emission measure. The factor a in this equation depends only weakly on electron temperature and frequency; it is tabulated for a wide range of frequencies and electron temperatures in Table 6 of Paper I. To compute the average value of the optical path length $\bar{\tau}_c$, we divide equation (6) of Paper I by T_e and substitute for the density distribution $N(\theta,\phi)$ the spherical Model I.[4] The evaluation of the integral yields equation (3). Hence the total flux density emitted by the optically thin spherical H II region is equal to the flux density emitted by a cylindrical H II region with the emission measure $E = D\theta_{\mathrm{sph}} N_0^2$ and the apparent diameter $\theta_{\mathrm{cyl}} = \frac{2}{3}\theta_{\mathrm{sph}}$.

At ν_t, the turnover frequency, $\bar{\tau}_c(\nu_t) = \frac{3}{2}$, and equation (3) consequently allows the computation of the emission measure if both T_e and ν_t are known.

$$\left(\frac{E_{\mathrm{center}}}{\mathrm{pc\ cm^{-6}}}\right) = \left(\frac{D}{\mathrm{pc}}\right)\left(\frac{\theta_{\mathrm{sph}}}{\mathrm{rad}}\right)\left(\frac{N_0}{\mathrm{cm^{-3}}}\right)^2 = a^{-1} \times 18.82 \left(\frac{T_e}{^\circ\mathrm{K}}\right)^{1.35} \left(\frac{\nu_t}{\mathrm{GHz}}\right)^{2.1}. \tag{A.2}$$

[4] Paper I, eq. (A 4), Model I should read $N_0^2\theta_{\mathrm{sph}}(1 - 4\theta^2/\theta^2_{\mathrm{sph}})^{1/2}$. Note, however, that this error is not contained in the subsequent equations of Paper I.

Knowing E, T_e, and the flux density S_ν at a frequency where $\tau_c \ll 1$, we can use equation (2*b*) of this paper to compute the source solid angle and, for the spherical model adopted here, the apparent diameter $\theta_{\rm sph}$ of the source

$$\left(\frac{\theta_{\rm sph}}{\rm rad}\right) = 2.74 \times 10^{-2} a^{-0.5} \left(\frac{T_e}{^\circ\rm K}\right)^{0.175} \left(\frac{\nu}{\rm GHz}\right)^{0.05} \left(\frac{E_{\rm center}}{\rm pc\ cm^{-6}}\right)^{-0.5} \left(\frac{S_\nu}{\rm f.u.}\right)^{0.5} \quad \text{(A.3)}$$

The electron density can be computed from $E_{\rm center}$ and $\theta_{\rm sph}$ if the distance D is known.

$$\left(\frac{N_0}{\rm cm^{-3}}\right) = 3.16 \times 10^{-2} \left(\frac{E_{\rm center}}{\rm pc\ cm^{-3}}\right)^{0.5} \left(\frac{D}{\rm kpc}\right)^{-0.5} \left(\frac{\theta_{\rm sph}}{\rm rad}\right)^{-0.5}. \quad \text{(A.4)}$$

The total mass of ionized hydrogen, expressed in solar masses, becomes

$$\frac{M_{\rm H\,II}}{M_\odot} = 1.29 \times 10^{7} \left(\frac{D}{\rm kpc}\right)^{3} \left(\frac{\theta_{\rm sph}}{\rm rad}\right)^{3} \left(\frac{N_0}{\rm cm^{-3}}\right). \quad \text{(A.5)}$$

TABLE 6

SPECTRUM OF A SPHERICAL H II REGION NEAR ITS TURNOVER FREQUENCY ν_t

τ_c	ν/ν_t	S_ν/S_ν''	S_ν''/S_ν for $\nu > \nu_t$ S'/S_ν for $\nu < \nu_t$
0.1	3.631	0.9635	1.038
0.3	2.152	.8960	1.116
0.5	1.687	.8351	1.197
0.7	1.438	.7801	1.282
0.9	1.275	.7304	1.369
1.1	1.159	.6853	1.459
1.3	1.071	.6443	1.552
1.5	1.000	.6070	1.647
1.7	0.9421	.5729	1.540
1.9	0.8935	.5418	1.457
2.1	0.8520	.5133	1.392
2.3	0.8158	.4872	1.339
2.5	0.7841	.4632	1.295
2.7	0.7559	.4410	1.260
2.9	0.7306	.4206	1.230
3.3	0.6870	.3843	1.183
3.7	0.6506	.3531	1.148
4.1	0.6195	.3260	1.122
4.5	0.5927	.3024	1.101
5.0	0.5637	.2770	1.083
6.0	0.5168	.2364	1.058
10.0	0.4052	.1470	1.020
15.0	0.3340	.0991	1.009
20.0	0.2913	.0746	1.005

To fit the model of a spherical H II region one determines the high- and low-frequency approximations S_ν' and S_ν'' of the observed spectrum and determines the turnover frequency ν_t from their intersection point. In the frequency range $3.63 \geq \nu/\nu_t > 0.41$, the approximations given by equations (2) deviate by more than 4 per cent from the true spectrum as given by the integral equation (1). In this frequency range the spectrum of the spherical H II region can be computed exactly using equation (4). For convenience we have evaluated equation (4) in a computer and tabulated its values in the third column of Table 6 as a function of both the optical depth τ_c (as defined by equation [3] and given in the first column), and the frequency ν (normalized to the turnover frequency ν_t and given in the second column). The values in the fourth column show by how much the approximations S_ν' and S_ν'' exceed the exact value S_ν.

REFERENCES

Akabane, K and Kerr, F. J. 1965, *Australian J. Phys.*, **18**, 91.
Baars, J. W. M., Mezger, P. G., and Wendker, H 1965, *Ap J* , **142**, 122.
Bennett, A. S 1962, *Mem R.A.S.*, **68**, 163
Burke, B. F., and Wilson, T. S. 1967, *Ap. J* , **150**, L13.
Burton, W B. 1966, Paper given at the 122d A A.S Meeting, Ithaca, N Y.
Cudaback, D. D , Read, R B., and Rougoor, G. W. 1966, *Phys Rev. Letters*, **17**, 452.
Davidson, K , and Harwit, M. 1967, *Ap J.*, **148**, 443.
Davies, R. D., Rowson, B., Booth, R. S., Cooper, A. J., Gent, H , Adgie, R. L., and Crowther, J H. 1967, *Nature*, **213**, 1109.
Ebert, R., Hoerner, S. von, and Temesvary, St 1960, *Die Entstehung von Sternen* (Berlin: Springer Verlag), p. 273.
Goldberg, L. 1966, *Ap. J* , **144**, 1225.
Gould, R. J., Gold, T., and Salpeter, E. E. 1963, *Ap. J.*, **138**, 408.
Mezger, P. G., Altenhoff, W., Schraml, J., Burke, B. F., Reifenstein, E. C , III, and Wilson, T L 1967, *Ap. J.* (*Letters*), **150**.
Mezger, P. G., and Henderson, A. P. 1967, *Ap J* , **147**, 471 (Paper I)
Mezger, P. G , and Höglund, B. 1967, *Ap. J* , **147**, 490 (Paper II).
Osterbrock, D. E. 1965, *Ap. J.*, **141**, 1285.
Pauliny-Toth, I. I. K., Wade, C. M., and Heeschen, D. S. 1966, *Ap J. Suppl* , **13**, 65.
Rogers, A E. E., Moran, J M., Crowther, P. P., Burke, B F , Meeks, M L , Ball, J A , and Hyde, G. M. 1966, *Phys Rev. Letters*, **17**, 450
——— 1967, *Ap. J.*, **147**, 360.
Ryle, M and Downes, D 1967, *Ap J* (*Letters*), **148**, L17
Sato, F , Akabane, K., and Kerr, F J. 1967, *Australian J. Phys.*, **20**, 197.
Shakeshaft, J R , Ryle, M , Baldwin, J. E , Elsmore, B , and Thomson, J. H 1955, *Mem R.A S* , **67**, 106.
Terzian, Yervant. 1965, *Ap J.*, **142**, 135
Weaver, H , Dieter, N. H and Williams, D R. W 1966 (as cited by Mezger and Höglund 1967)
Westerhout, G 1958, *B A N* , **14**, 215.
Wilson, T L , Reifenstein, E C , III, Burke, B F , and Mezger, P G 1967, Paper given at the URSI Spring Meeting in Ottawa, Canada, May 24, 1967